

# Optical needles with arbitrary homogeneous three-dimensional polarization

Li Hang, Ying Wang, and Peifeng Chen \*

School of Optical and Electronic Information, Huazhong University of Science and Technology, Wuhan, China

## Abstract

we propose a new method to generate optical needles by focusing vector beams comprised of radially polarized component and azimuthally polarized vortex components. The radial part can generate longitudinal polarization, while the azimuthal parts can generate left- and right-handed polarization. Hence, an arbitrary 3D polarization can be obtained. To our knowledge, it may be the first time that arbitrarily polarized optical needles whose transverse sizes are under  $0.5\lambda$  have been achieved. And their polarized homogeneity is beyond 0.97.

## 1 Introduction

Over the past few years, there are several papers about generating optical fields with three-dimensional polarization by tightly focusing [1–3]. However, they do not show a quantitative relationship between the input field and the three-dimensional polarization of the focal field. In this paper, we propose a new method to generate super-resolved optical fields by focusing complex input field. Such optical fields have large longitudinal full width at half maximum (LFWHM) and small transverse full width at half maximum (TFWHM), so they are called optical needles [4, 5]. The input field comprise radially polarized beam and azimuthally polarized vortex beams. The radially polarized beam can generate the longitudinally polarized field [6], while the azimuthally polarized beams with vortex phase  $\exp(\pm i\varphi)$  can generate left- and right-handed polarized fields. These three components constitute three-dimensional unitary bases. Thus, an arbitrary polarization can be obtained.

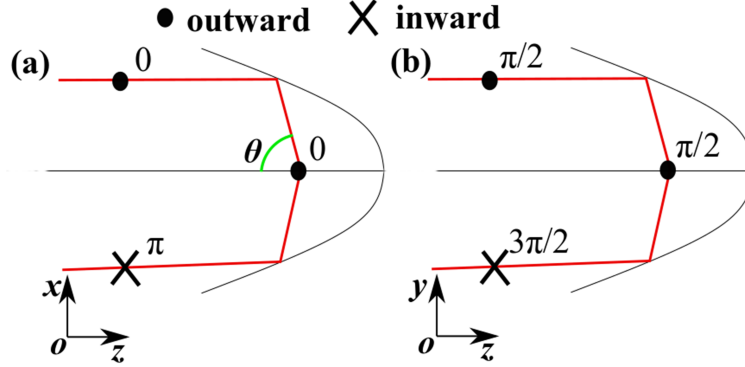


Figure 1: Schematic diagrams of an azimuthally polarized beam with vortex phase  $\exp(i\varphi)$  generating a left-handed polarized beam. (a) in  $xOz$  plane; (b) in  $yOz$  plane.

## 2 Theory and configuration

Figure 1 shows how an azimuthally polarized beam with vortex phase  $\exp(i\varphi)$  generates a left-handed polarized beam. The dots and crosses are the directions of the electric field when the phases are not considered. The numbers near the dots and crosses are the phases of the electric fields. In Fig. 1(a), the electric field near the focus is parallel to  $y$ -axis, while in Fig. 1(b) it is parallel to  $x$ -axis. Since there is a phase retardation of  $\pi/2$ , the total field is left-handed polarized. Similarly, the focal field will be right-handed polarized when the incident beam is azimuthally polarized with vortex phase  $\exp(-i\varphi)$ . In fact, this is an example of orbital-to-spin conversion [7,8]. An annular input beam comprised of radially polarized component and azimuthally polarized vortex can be expressed as

$$\mathbf{E}_{in} = \begin{cases} = f\mathbf{e}_r + g_{-1}\exp(-i\varphi)\mathbf{e}_\varphi + g_1\exp(i\varphi)\mathbf{e}_\varphi, & |\theta - \theta_0| \leq \Delta\theta/2 \\ = 0, & |\theta - \theta_0| > \Delta\theta/2, \end{cases} \quad (1)$$

where  $\theta_0$  and  $\Delta\theta$  are the angular position and width of the incident beam. Such beams can be generated by spatial light modulators [9,10]. For a parabolic mirror in Fig. 1,  $\theta_0 = 90^\circ$  is chosen in this paper.  $f$ ,  $g_{-1}$  and  $g_1$  are complex numbers. According to the Richards-Wolf vector diffraction theory [11], when  $\Delta\theta \ll \theta_0$ , the electric field near the focus can be expressed as [12]

\*Corresponding author: pfchen@hust.edu.cn Li Hang: lihng5011@vip.qq.com

$$\begin{aligned}\mathbf{E}(r, \phi, z) &\approx \frac{A(z; \theta_0, \lambda)}{\sqrt{2}} \begin{bmatrix} -ig_{-1}(e^{-2i\phi} J_2 + J_0)\mathbf{e}_x + ig_1(e^{2i\phi} J_2 + J_0)\mathbf{e}_x \\ g_{-1}(e^{-2i\phi} J_2 - J_0)\mathbf{e}_y + g_1(e^{2i\phi} J_2 - J_0)\mathbf{e}_y \\ 2fJ_0\mathbf{e}_z \end{bmatrix} \\ &= A(z) \begin{bmatrix} i(-g_{-1}J_0 + g_1e^{2i\phi} J_2)\mathbf{e}_R \\ i(g_1J_0 - g_{-1}e^{-2i\phi} J_2)\mathbf{e}_L \\ \sqrt{2}fJ_0\mathbf{e}_z \end{bmatrix},\end{aligned}\quad (2)$$

where  $A(z) \propto \frac{\sin(kz \sin \frac{\delta\theta}{2})}{kz}$ ,  $k$  is wave number.  $J_n = J_n(kr)$ , where  $J_n(\cdot)$  denotes the  $n$ th-order Bessel function of the first kind.  $\mathbf{e}_R = (\mathbf{e}_x - i\mathbf{e}_y)/\sqrt{2}$  and  $\mathbf{e}_L = (\mathbf{e}_x + i\mathbf{e}_y)/\sqrt{2}$  represent the unit vector of right- and left-handed circular polarization states, respectively. Obviously, the focal field is a non-diffracting beam. Its LFWHM is  $0.8713\lambda/\Delta\theta$  [12, 13]. Its TFWHM can be obtained by solving the equation

$$|\mathbf{E}(r, \phi, z)|^2 = |\mathbf{E}(0, 0, z)|^2/2. \quad (3)$$

The TFWHM is dependent on  $\phi$  and the numerical results are shown in the next section. The electrical field strength at the focus is  $\mathbf{E}_0 = \mathbf{E}(0, 0, 0) = -ig_{-1}\mathbf{e}_R + ig_1\mathbf{e}_L + \sqrt{2}f\mathbf{e}_z$  ( $A(z)$  will be omitted in the following). To evaluate the polarized homogeneity near the focus quantitatively, we can define polarized homogeneity as

$$\eta = \frac{\int_S |\mathbf{E}^* \cdot \frac{\mathbf{E}_0}{|\mathbf{E}_0|}|^2 dS}{\int_S \mathbf{E}^* \cdot \mathbf{E} dS}, \quad (4)$$

where  $S$  is the integral area in the focal plane. Considering a circular area  $r < R$ , the polarized homogeneity can be simplified as

$$\eta = \frac{\int_0^R [(\alpha^2 + \beta^2 + 2\gamma^2)^2 J_0^2 + 2\alpha^2\beta^2 J_2^2] r dr}{\int_0^R [(\alpha^2 + \beta^2 + 2\gamma^2)^2 J_0^2 + (\alpha^2 + \beta^2 + 2\gamma^2)(\alpha^2 + \beta^2) J_2^2] r dr} \quad (5)$$

with

$$\begin{aligned}\alpha &= |g_{-1}|/\sqrt{|g_{-1}|^2 + |g_1|^2 + |f|^2} \\ \beta &= |g_1|/\sqrt{|g_{-1}|^2 + |g_1|^2 + |f|^2} \\ \gamma &= |f|/\sqrt{|g_{-1}|^2 + |g_1|^2 + |f|^2},\end{aligned}\quad (6)$$

where  $\alpha$ ,  $\beta$  and  $\gamma$  represent the weighting factors of the three components of the incident beam. Only when  $\alpha = \beta = 0$ ,  $\eta = 1$ . This is because the azimuthally polarized beams with vortex phase  $\exp(\pm i\varphi)$  cannot be transformed into left- or right-handed polarized beams completely.

## 3 Numerical simulation and discussion

### 3.1 TFWHM

Substituting Eq. (2) and Eq. (6) into Eq. (3),

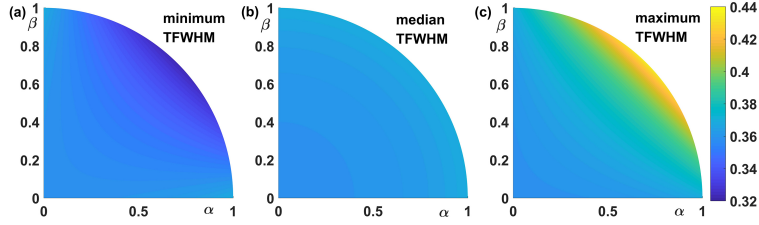


Figure 2: Minimum (a), median and maximum (c) TFWHM as functions of  $\alpha$  and  $\beta$ .

$$\begin{aligned}
 & (\alpha^2 + \beta^2 + 2\gamma^2)J_0^2 + (\alpha^2 + \beta^2)J_2^2 - 2\alpha\beta \cos(\delta_1 - \delta_2 - 2\phi)J_0J_2 \\
 & = (\alpha^2 + \beta^2 + 2\gamma^2)/2, \tag{7}
 \end{aligned}$$

where  $\delta_1$  and  $\delta_2$  are the complex arguments of  $g_{-1}$  and  $g_1$ , respectively. Equation 7 shows that TFWHMs will be dependent on  $\phi$  unless  $\alpha\beta = 0$ . Because of the interaction of the two azimuthally polarized components, the focal spot is not a circle, but like an ellipse. Hence, we use minimum (when  $\delta_1 - \delta_2 - 2\phi = \pi$ ), median (when  $\delta_1 - \delta_2 - 2\phi = \pi/2$ ) and maximum (when  $\delta_1 - \delta_2 - 2\phi = 0$ ) TFWHM to evaluate the size of focal spots. As shown in Fig. 2, their ranges are  $0.32 \sim 0.37\lambda$ ,  $0.36 \sim 0.37\lambda$  and  $0.36 \sim 0.43\lambda$ , respectively. When  $\alpha^2 = \beta^2 = 0.5$ , the influence of the two azimuthally polarized components reaches the maximum, so the focal spot has the minimum value of minimum TFWHMs ( $0.32\lambda$ ) and the maximum value of maximum TFWHMs ( $0.43\lambda$ ). Median TFWHMs are only dependent on  $\gamma$ . The radially polarized component only generate zero-order Bessel component, while the azimuthally polarized components can both generate zero- and second-order Bessel component. Therefore, the median TFWHM increase as  $\gamma$  decrease.

### 3.2 Polarized homogeneity

According to Eq. (5), the polarized homogeneity is shown in Fig. 3. It is always larger than 0.989 when  $R = 0.185\lambda$  and larger than 0.977 when  $R = 0.22\lambda$ . It increases as  $\gamma$  increases because of the incomplete transformation of the azimuthally polarized components. For a fixed  $\gamma$ , the maximum polarized homogeneity is at  $\alpha = \beta$ . This is because the bad transformation of two azimuthally polarized components can cancel partly.

### 3.3 Examples

That  $\mathbf{E}_0$  is linearly polarized is equivalent to  $\mathbf{E}_0 \times \mathbf{E}_0^* = \mathbf{0}$ . Figure 4 is an example when  $g_{-1} = g_1 = f$ . The  $x$ -component of electric field is nearly zero and the  $y$ -component and  $z$ -component have a phase retardation of  $\pi$ . Hence, the focal field is linearly polarized in  $yOz$  plane. The minimum, median and maximum

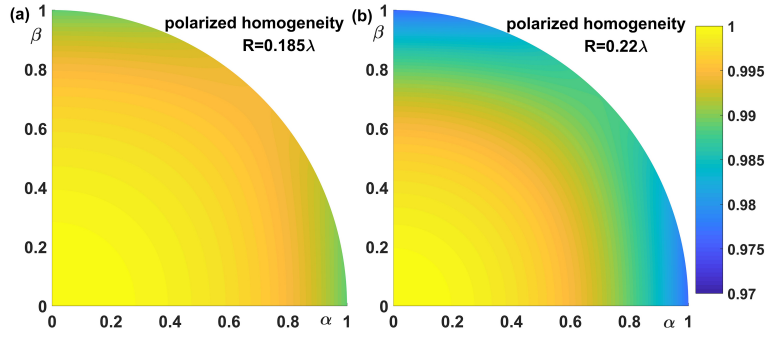


Figure 3: Polarized homogeneity as functions of  $\alpha$  and  $\beta$ . (a) and (b) correspond to median and maximum TFWHM, respectively.

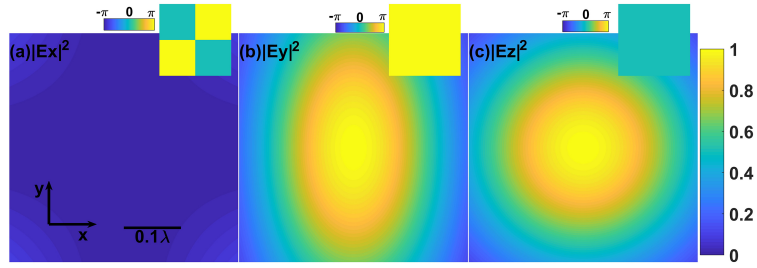


Figure 4: Intensity and phase (insets) profiles on the focal plane when  $g_{-1} = g_1 = f$ .

TFWHM are  $0.34$ ,  $0.36$  and  $0.39\lambda$ , respectively. The polarized homogeneity is  $0.991$  ( $R=0.22\lambda$ ).

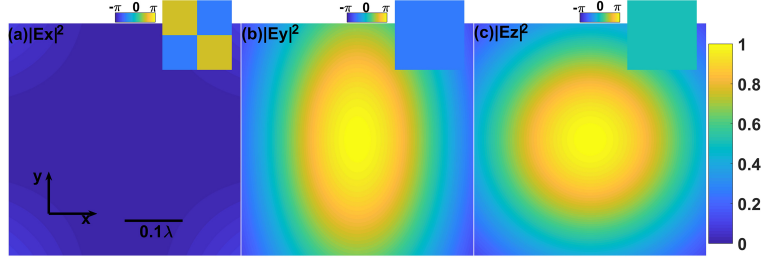


Figure 5: Intensity and phase (insets) profiles on the focal plane when  $g_{-1} = g_1 = if$ .

That  $\mathbf{E}_0$  is circularly polarized is equivalent to  $|\mathbf{E}_0 \times \mathbf{E}_0^*| = \mathbf{E}_0 \cdot \mathbf{E}_0^*$ . Figure 5 is an example when  $g_{-1} = g_1 = if$ . Compared with last example, the azimuthally polarized components have phases of  $\pi/2$ . The intensity profiles in Fig. 5 are the same as Fig. 4, while the phase retardation between y-component and z-component of the focal field is  $\pi/2$ . Hence, the focal field is circularly polarized in  $yOz$  plane.

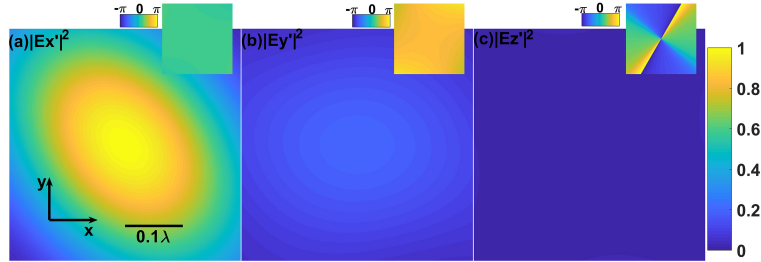


Figure 6: Intensity and phase (insets) profiles on the focal plane when  $f = -ig_{-1} = g_1/\sqrt{3}$ .

Figure 6 is an example of elliptical polarization with  $f = -ig_{-1} = g_1/\sqrt{3}$ . In order to display the polarization clearly, we use an orthogonal transformation:

$$\begin{bmatrix} E_{x'} \\ E_{y'} \\ E_{z'} \end{bmatrix} = \begin{bmatrix} \frac{\sqrt{3}}{\sqrt{10}} & \frac{-2}{\sqrt{10}} & \frac{\sqrt{3}}{\sqrt{10}} \\ \frac{1}{\sqrt{2}} & \frac{0}{\sqrt{2}} & \frac{-1}{\sqrt{2}} \\ \frac{1}{\sqrt{5}} & \frac{\sqrt{3}}{\sqrt{5}} & \frac{1}{\sqrt{5}} \end{bmatrix} \begin{bmatrix} E_x \\ E_y \\ E_z \end{bmatrix}. \quad (8)$$

As shown in Fig. 6,  $|E_{z'}|^2$  is nearly zero. The phase retardation between  $x'$ -component and  $y'$ -component are about  $\pi/2$ , but their amplitudes are different. So the focal field is elliptically polarized. The minimum, median and maximum TFWHM are  $0.34$ ,  $0.37$  and  $0.40\lambda$ , respectively. The polarized homogeneity is  $0.988$  ( $R=0.22\lambda$ ).

## 4 Conclusion

In conclusion, we presented an approach to generate an arbitrary 3D polarization by tightly focusing vector beams. The size of the focal spots is  $0.32 \sim 0.44\lambda$ . The polarized homogeneity is always large than 0.97.

## References

- [1] Ayman F Abouraddy and Kimani C Toussaint Jr. Three-dimensional polarization control in microscopy. *Physical Review Letters*, 96(15):153901, 2006.
- [2] Weibin Chen and Qiwen Zhan. Diffraction limited focusing with controllable arbitrary three-dimensional polarization. *Journal of Optics*, 12(4):045707, 2010.
- [3] Wenguo Zhu and Weilong She. Generation of tunable three-dimensional polarization in 4pi focusing system. *Optics Express*, 21(14):17265–17274, 2013.
- [4] D Panneton, G St-Onge, M Piché, and S Thibault. Needles of light produced with a spherical mirror. *Optics Letters*, 40(3):419–422, 2015.
- [5] Li Hang, Ying Wang, and Peifeng Chen. Needles of light produced with a quasi-parabolic mirror. *Journal of the Optical Society of America A*, 35(1):174–178, 2018.
- [6] Qiwen Zhan. Cylindrical vector beams: from mathematical concepts to applications. *Advances in Optics and Photonics*, 1(1):1–57, 2009.
- [7] Panpan Yu, Qian Zhao, Xinyao Hu, Yinmei Li, and Lei Gong. Orbit-induced localized spin angular momentum in the tight focusing of linearly polarized vortex beams. *Optics Letters*, 43(22):5677–5680, 2018.
- [8] Li Hang, Ying Wang, and Peifeng Chen. Symmetry of electric spin angular momentum density in the tight focusing of linearly polarized vortex beams. *J. Opt. Soc. Am. A*, 36(8):1374–1378, Aug 2019.
- [9] Wei Han, Yanfang Yang, Wen Cheng, and Qiwen Zhan. Vectorial optical field generator for the creation of arbitrarily complex fields. *Optics Express*, 21(18):20692–20706, 2013.
- [10] Carmelo Rosales-Guzmán, Nkosiphile Bhebhe, and Andrew Forbes. Simultaneous generation of multiple vector beams on a single slm. *Optics Express*, 25(21):25697–25706, 2017.
- [11] B Richards and E Wolf. Electromagnetic diffraction in optical systems, ii. structure of the image field in an aplanatic system. *Proc. R. Soc. Lond. A*, 253(1274):358–379, 1959.

- [12] Li Hang, Peifeng Chen, and Ying Wang. Theoretical generation of arbitrarily homogeneously 3d spin-orientated optical needles and chains. *Optics Express*, 27(5):6047–6056, 2019.
- [13] Li Hang, Kaixi Huang, Jian Fu, Ying Wang, and Peifeng Chen. Tunable magnetization chains induced with annular parabolic mirrors. *IEEE Photonics Journal*, 10(5):1–7, 2018.